Collagen scaffold combined with human umbilical cord-mesenchymal stem cells transplantation for acute complete spinal cord injury

Wu-Sheng Deng[1, #], Ke Ma[2, #], Bing Liang[2, #], Xiao-Yin Liu[3], Hui-You Xu[2], Jian Zhang[2], Heng-Yuan Shi[4], Hong-Tao Sun[2], Xu-Yi Chen[2, *], Sai Zhang[2, *]

1 College of Integrated Traditional Chinese and Western Medicine, Gansu University of Chinese Medicine, Lanzhou, Gansu Province, China
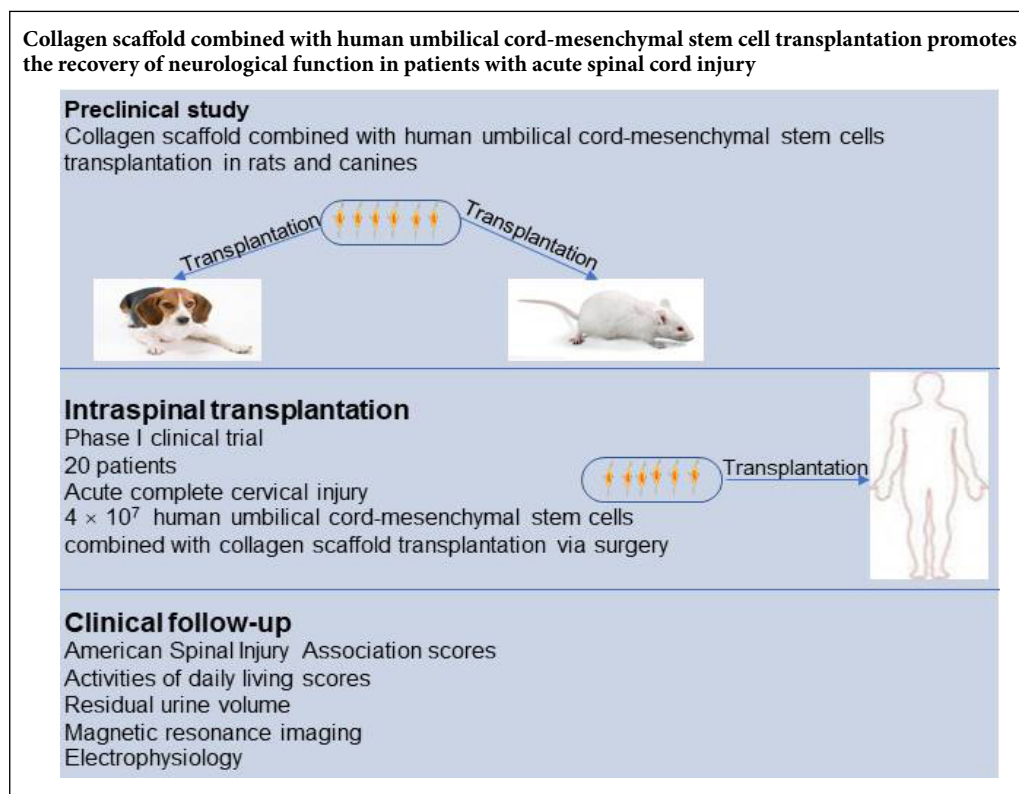2 Tianjin Key Laboratory of Neurotrauma Repair, Pingjin Hospital Brain Center, characteristic medical center of Chinese people's armed police force, Tianjin, China
3 Clinical School of Medicine, Tianjin Medical University, Tianjin, China
4 Clinical School of Medicine, Logistics University of People's Armed Police Force, Tianjin, China

Graphical Abstract

Collagen scaffold combined with human umbilical cord-mesenchymal stem cell transplantation promotes the recovery of neurological function in patients with acute spinal cord injury

Preclinical study
Collagen scaffold combined with human umbilical cord-mesenchymal stem cells transplantation in rats and canines

Transplantation — Transplantation

Intraspinal transplantation
Phase I clinical trial
20 patients
Acute complete cervical injury
4×10^7 human umbilical cord-mesenchymal stem cells combined with collagen scaffold transplantation via surgery

Transplantation

Clinical follow-up
American Spinal Injury Association scores
Activities of daily living scores
Residual urine volume
Magnetic resonance imaging
Electrophysiology

Correspondence to:
Sai Zhang, MD, PhD,
zhangsai718@vip.126.com;
Xu-Yi Chen, MD, PhD,
chenxuyi1979@126.com.

#These authors contributed equally to this work.

orcid:
0000-0002-8028-4183
(Sai Zhang)
0000-0002-0420-8349
(Xu-Yi Chen)

Abstract

Currently, there is no effective strategy to promote functional recovery after a spinal cord injury. Collagen scaffolds can not only provide support and guidance for axonal regeneration, but can also serve as a bridge for nerve regeneration at the injury site. They can additionally be used as carriers to retain mesenchymal stem cells at the injury site to enhance their effectiveness. Hence, we hypothesized that transplanting human umbilical cord-mesenchymal stem cells on collagen scaffolds would enhance healing following acute complete spinal cord injury. Here, we test this hypothesis through animal studies and a phase I clinical trial. (1) Animal experiments: Models of completely transected spinal cord injury were established in rats and canines by microsurgery. Mesenchymal stem cells derived from neonatal umbilical cord tissue were adsorbed onto collagen scaffolds and surgically implanted at the injury site in rats and canines; the animals were observed after 1 week–6 months. The transplantation resulted in increased motor scores, enhanced amplitude and shortened latency of the motor evoked potential, and reduced injury area as measured by magnetic resonance imaging. (2) Phase I clinical trial: Forty patients with acute complete cervical injuries were enrolled at the Characteristic Medical Center of Chinese People's Armed Police Force and divided into two groups. The treatment group (*n* = 20) received collagen scaffolds loaded with mesenchymal stem cells derived from neonatal umbilical cord

tissues; the control group (*n* = 20) did not receive the stem-cell loaded collagen implant. All patients were followed for 12 months. In the treatment group, the American Spinal Injury Association scores and activities of daily life scores were increased, bowel and urinary functions were recovered, and residual urine volume was reduced compared with the pre-treatment baseline. Furthermore, magnetic resonance imaging showed that new nerve fiber connections were formed, and diffusion tensor imaging showed that electrophysiological activity was recovered after the treatment. No serious complication was observed during follow-up. In contrast, the neurological functions of the patients in the control group were not improved over the follow-up period. The above data preliminarily demonstrate that the transplantation of human umbilical cord-mesenchymal stem cells on a collagen scaffold can promote the recovery of neurological function after acute spinal cord injury. In the future, these results need to be confirmed in a multicenter, randomized controlled clinical trial with a larger sample size. The clinical trial was approved by the Ethics Committee of the Characteristic Medical Center of Chinese People's Armed Police Force on February 3, 2016 (approval No. PJHEC-2016-A8). All animal experiments were approved by the Ethics Committee of the Characteristic Medical Center of Chinese People's Armed Police Force on May 20, 2015 (approval No. PJHEC-2015-D5).

Key Words: *canine; collagen scaffolds; human; human umbilical cord-mesenchymal stem cells; nerve regeneration; rat; spinal cord injury*

Chinese Library Classification No. *R459.9; R363; R364*

Introduction

The restoration of function following complete spinal cord injury (SCI) is increasingly considered to be one of the most challenging global health problems (Maier and Schwab, 2006; Ghatas et al., 2018; Brown and Martinez, 2019; Sun et al., 2020). SCI not only has a tremendous adverse impact on a patient's psychology, but also brings about considerable economic burdens: personal, family, and society (Selvarajah et al., 2014). To date, although therapeutic strategies for SCI can extend the lifespan of patients, therapies for promoting neurological recovery following SCI are largely ineffective (Harness et al., 2008; García-Altés et al., 2012).

In the acute phase of an SCI, the initial direct trauma leads to tissue damage involving blood vessels and cell membranes. Then, subacute damage is triggered, including hemorrhage, ischemia, edema, excitotoxicity, inflammation, free radical production, and necrosis and apoptosis of nerve cells (Fitch and Silver, 2008; David et al., 2012). The failure of nerve regeneration in the adult central nervous system may be attributed to several mechanisms, including the absence of regenerative neurons at the injury site, difficulty in regenerating myelin, lack of various growth factors or neurotrophic stimulation, deficiency of suitable matrices to sustain and guide axonal extension at the lesion site, and formation of necrotic tissues and glial scarring in the acute or chronic injured spinal cord (Schwab and Brösamle, 1997; Profyris et al., 2004; Properzi et al., 2005; Kadoya et al., 2009).

Many preclinical experiments have shown that mesenchymal stem cell-based therapies are some of the most promising clinical approaches for SCI. There are various sources of MSCs, such as bone marrow, the umbilical cord, and adipose tissue. In particular, human umbilical cord-mesenchymal stem cells (hUC-MSCs) offer several advantages: they can be obtained without inflicting pain on the donor, they are associated with minimal ethical controversy compared to embryonic stem cells, and they exhibit faster self-renewal characteristics than other stem cells, such as adipose-derived mesenchymal stem cells, and bone marrow-derived mesenchymal stem cells (Hu et al., 2010). Moreover, as hUC-MSCs are immunoprivileged, they express limited major histocompatibility complex class II and costimulatory molecules, making them suitable for transplantation. Furthermore, they

can modulate the immune response upon transplantation via cell-cell interactions and by modulation immune cell functions (De Miguel et al., 2012). In addition, MSCs inhibit astrogliosis and microglial activation, inflammatory, and angiogenic effects, which are advantageous for SCI therapy (Cízková et al., 2006; Ruff et al., 2012; Ritfeld et al., 2015; Noh et al., 2016).

Collagen scaffolds (CSs) have been widely used as biomaterials for SCI treatment (Liu et al., 2012; Han et al., 2014; Li et al., 2016; Snider et al., 2017; Zhang et al., 2019). CSs offer considerable advantages for this application, including low antigenicity, excellent biocompatibility, and good biodegradability (Han et al., 2009; Fan et al., 2010; Li et al., 2017a; Wang et al., 2018). In previous studies, CSs have been tested using rat models with completely transected spinal cords and have been found to reduce the lesion area, support cell migration, guide the orderly regeneration of nerve fibers, and direct axon elongation, all of which promote the recovery of neurological function (Li et al., 2016; Xu et al., 2017; Wang et al., 2018). These experimental results were further verified in dog models with complete spinal cord transection (Lin et al., 2006; Han et al., 2009, 2010, 2015; Li et al., 2016). These results in animal models suggest that implanting CSs into the lesion site may be effective for treating SCI.

In this study, we conducted animal experiments to assess the effects of transplanting hUC-MSCs in a CS on functional recovery in rats and dogs with completely transected spinal cords. Then, we carried out a clinical trial to evaluate the safety and efficacy of the hUC-MSC-laden CS transplanted into the injured spinal cords of patients diagnosed with acute complete cervical SCI. Zhao et al. (2017) reported that the transplantation of a CS loaded with hUC-MSCs in chronic SCI patients promoted functional recovery. However, in our phase I clinical trial, the control group was designed, and quantitative DTI analysis was performed, so the results provide stronger evidence that the application of a hUC-MSC-laden CS can improve neurological function.

Materials/Subjects and Methods
Pre-clinical studies
CS preparation
The CS was prepared from bovine aponeurosis using previ-

ously reported methods (Lin et al., 2006; Xiao et al., 2016). Briefly, fresh bovine aponeuroses were obtained from a slaughterhouse (Wanlifa, Beijing, China) and repeatedly rinsed with cold distilled water. Connective tissue, fat, and residual muscles were removed. The samples were repeatedly rinsed to thoroughly remove the residual tissues and freeze-dried. The product was a standard CS that was used in all experiments. The biological safety aspects of the CS, including its acute toxicity, chronic toxicity, cytotoxicity, genetic toxicity, hemolytic toxicity, intradermal irritation, allergen detection, and degradability, were evaluated by the National Institute for Food and Drug Control according to the Chinese Criterion for Medical Devices GB16886.

Isolation, culture, and identification of human umbilical cord-mesenchymal stem cells

hUC-MSCs were derived from the umbilical cord of a human donor (37–42 weeks of gestation). The umbilical cord was obtained without adverse effects on either the pregnant women or the neonate. The harvest of the human umbilical cord was approved by the Characteristic Medical Center of Chinese People's Armed Police Force (approval No. PJLEC-2016-R8), and consent was obtained from the mother and her family. hUC-MSCs were isolated, cultured, and identified as described previously (Tu et al., 2012; Zhao et al., 2017). Briefly, two arteries and one vein were dissected. The blood and epidermal tissues were removed. The remaining Wharton's jelly was cut into 1–2 cm^2 pieces and successively digested with collagenase (Solarbio Science & Technology Co., Ltd., Beijing, China) and 0.25% trypsin (Solarbio Science & Technology Co., Ltd.) at 37°C for 18 hours. The undigested tissue was then removed using a 100 μm filter to procure a cell suspension. This cell suspension was seeded in Dulbecco's modified eagle's medium (DMEM/F12; Thermo Fisher Scientific Co., Ltd., Shanghai, China) containing 20% fetal bovine serum (MRC Biotechnology Co., Ltd., Jiangsu, China), 2 mM glutamine (Sigma-Aldrich, St. Louis, MO, USA), and 100 U of penicillin and streptomycin (Solarbio Science & Technology Co., Ltd.). Cells were incubated in a 37°C, 5% CO$_2$ incubator. The medium was replaced after 3 days of incubation to remove non-adherent cells. Thereafter, the medium was changed twice weekly. The cells were passaged when they reached 80% confluence.

To prepare the cells for transplantation, 4×10^7 cells were aliquoted, and the hUC-MSCs were identified by flow cytometry (Beckman Coulter, Brea, CA, USA) with antibodies against CD105, CD73, CD90, and human leukocyte antigen-antigen D related (HLA-DR; Abcam, Cambridge, UK). Hence, approximately 4×10^7 hUC-MSCs were identified from the aliquot.

hUC-MSCs were seeded on the CS and allowed to adsorbed over 7 days of incubation. After the co-culture period, the growth of the hUC-MSCs was observed under an inverted phase-contrast microscope (Boshida Optical Instrument, Shenzhen, China). In addition, the CS was fixed, dehydrated, dried, and coated with gold, and the hUC-MSC morphology was examined under a scanning electron mi-

croscope (Hitachi, Tokyo, Japan). The CS was maintained pathogen- and virus-free and throughout the preparation, and bacterial endotoxin testing was performed.

Scaffold biocompatibility

The prepared CS was sterilized by ^{60}Co irradiation, placed in 24-well plates, and incubated overnight in low-sugar DMEM containing 10% fetal bovine serum (MRC Biotechnology Co., Ltd.). hUC-MSCs at passage 3 were placed in the wells containing prepared CS at a density of 1×10^5/well and cultured in a 37°C, 5% CO$_2$ incubator. Routine adherent cell culture was used for the control group without CS. Five replicate wells were prepared in each group. The medium was removed after 1, 3, 5, and 7 days after transferring to the well plates and carefully washed twice in phosphate-buffered saline (PBS). Then, serum-free medium containing 10% CCK-8 reagent (Solarbio Science & Technology Co., Ltd.) was added to each well and incubated for an additional 2 hours. Next, 100 μL of the solution was transferred from each well and into a 96-well plate to measure the optical density (OD) at 450 nm using a microplate reader (Thermo Fisher Scientific, Waltham, MA, USA). Thus, the OD values reflect cell proliferation over the culture period. The OD values of five replicate wells were averaged.

At 7 days of incubation on the CS, the growth of the hUC-MSCs was observed under an inverted phase-contrast microscope. In addition, the CS was fixed, dehydrated, and coated with gold, and the hUC-MSC morphology and growth were observed on a scanning electron microscope (Hitachi, Tokyo, Japan).

Animals

Forty female specific-pathogen-free Sprague-Dawley rats weighing 250–300 g and aged 8 weeks were supplied by the Military Academy of Medical Sciences of Chinese People's Liberation Army (animal license No. SYXK (Jing) 2018-0013; animal batch No. 2018-0026.7). The rats were normally housed in controlled animal quarters at room temperature in the range of 18–22°C and relative humidity between 50% and 60%, with fluorescent light lighting on 12-hour day and night.

Twenty healthy female beagle canines aged 1 year old and weighing 11–14 kg were supplied b Beijing Fangyuanyuan Animal Center, China (animal license No. SCXK (Jing) 2018-0026; animal batch No. 12425316725936). The canines were fed in single cages with laminar flow purification. The room temperature was maintained in the range of 22–23°C and the relative humidity was in the range of 40–45%.

The animal experiments were approved by the Ethics Committee of Characteristic Medical Center of Chinese People's Armed Police Force on May 20, 2015 (approval No. PJHEC-2015-D5). The animals were fed in the Experimental Animal Center of Characteristic Medical Center of Chinese People's Armed Police Force. The animals were allowed free access to food and water. After successful model establishment, an air cushion was placed at the bottom of the cage to prevent pressure sores.

Spinal cord injury and transplantation

Rats were randomly divided into the sham group (receiving the hUC-MSC-laden CS without SCI, $n = 10$), SCI group (receiving spinal cord transection without hUC-MSC/CS treatment, $n = 10$), CS group (receiving spinal cord transection followed by implantation of the CS, $n = 10$), and CS + hUC-MSCs group (receiving spinal cord transection followed by implantation of the hUC-MSC-laden CS, $n = 10$).

All rats were anesthetized by intraperitoneal injection with 1% sodium pentobarbital (40 mg/kg; Sigma-Aldrich) to prevent infection. Under an operation microscope, the skin and muscles were opened, and the paravertebral muscles were dissected away to expose the spinous processes and lamina of T9, T10, and T11. Following laminectomy at the levels of T9 to T11, the spinal cord was exposed. A 1.5 mm-long section of the spinal cord at the T10 level was cut using microsurgical scissors and removed (**Figure 1A**). Immediately after the SCI, a 4-mm-diameter CS was implanted into the completely transected gap of the CS group, and a 1×10^6 hUC-MSC-laden CS was implanted into the completely transected gap of the CS + hUC-MSCs group (**Figure 1B**). The subcutaneous tissue and skin incisions were sutured layer-by-layer. The hind limbs of the rats were immediately paralyzed, demonstrating that the model was successful. After the operation, the bladder was squeezed twice daily until the bladder function was recovered. Hindlimb motor function, wound condition, and food and water intake were noted daily. The wound was disinfected with iodophor, and 200,000 units of penicillin were injected intramuscularly every day for 7 days following surgery.

A similar procedure was also conducted in canines. Twenty canines were randomly divided into sham group (Only exposing the spinal cord without SCI, $n = 5$), SCI group (receiving spinal cord transection without hUC-MSC/CS treatment, $n = 5$), CS group (receiving spinal cord transection followed by implantation of the CS, $n = 5$), and CS + hUC-MSCs group (receiving spinal cord transection followed by implantation of the hUC-MSC-laden CS, $n = 5$).

All canines underwent preoperative fasting for 12 hours. The canines were subcutaneously administered atropine sulfate (0.025 mg/kg; Roche Group, WuHan, China) 30 minutes before anesthesia. The animals were anesthetized by intravenous propofol administration (7 mg/kg; Fresenius Kabi AB, Baden Humboldt, Germany) followed by isoflurane anesthesia by inhalation (volume concentration 2.0%, oxygen flow 2 L/min; RuiTaibio, Beijing, China). The anesthetized canines were placed in a prone position, and their limbs were fixed, and the hair on the back of each animal was shaved. Blood pressure, heart rate, pulse, oxygen saturation, body temperature, and other vital signs were monitored. The skin and subcutaneous tissue were cut with a posterior median straight incision (T8–11) to expose the lamina, the spinous processes at T8–11 were dissected out, and a laminectomy was performed at T8–11 levels (**Figure 1C**). The dura mater of T8–11 was cut longitudinally with an approximately 1.5 cm incision to expose the spinal cord (**Figure 1D**). A 3 mm-long section of the spinal cord at T8–11 levels was completely transected using microsurgical scissors, neurosurgical bipolar forceps, and suction (**Figure 1E**). After complete hemostasis, a 5 mm-diameter, 3 mm-long CS was implanted in the gap in the spinal cord for the CS group, and the CS co-cultured with 1×10^7 hUC-MSCs was implanted for the CS + hUC-MSCs group (**Figure 1F**). The dura mater was sutured tightly, and the paraspinal muscles and skin were sutured separately and bandaged. The loss of motor function (i.e., both hind limbs of each canine were paralyzed) indicated successful model establishment. The beagles were kept in the laboratory animal room with suitable temperature and humidity. The bladder of each animal was squeezed six times per day using the method described by Crede (Momose et al., 1997). Catheters were placed in any beagles exhibiting dysuria until spontaneous urination was restored. As a prophylactic against infection, the beagles were given intramuscular injections of gentamicin (80,000 units/day; Solarbio Science & Technology Co., Ltd.) every day for 7 days following the procedure. Ringer's lactate solution (200 mL/day) (Sigma-Aldrich) was administered intravenously once each day for 3 days after surgery to prevent complications such as hypothermia and hypotension.

Behavioral assessment

Locomotor function was assessed in a double-blind manner for each rat before surgery and 1, 2, 3, 4, 6, and 8 weeks after surgery. The rats were individually observed and recorded for 5 minutes by two laboratory workers (Basso et al., 1995) and rated on the 21-point Basso-Beattie-Bresnahan (BBB) locomotor rating scale. Higher BBB scores imply better recovery of motor function. The modified Rivlin slope experiment (Rivlin and Tator, 1977) was also performed, and the highest angle of inclination was defined as that which could be maintained for 5 seconds. Each animal underwent this assessment five times, and the average measurement was recorded.

Locomotor function was assessed in canines before surgery and at 0.5, 1, 2, 3, 4, 5, and 6 months after surgery. The canines were placed in an open area and allowed to move freely; the animals were individually recorded, and the captured videos were evaluated in a double-blind manner. The Olby scoring system (Olby et al., 2001) was used to assess the automatic and non-automatic movements of the hindlimbs in terms of the joint movement, deep pain reflex, muscle strength, weight-bearing capacity, and gait. The scores were on a scale from 0 to 15, with 15 points representing the best recovery of motor function. The score was measured three times. The mean score was taken as the result.

Evaluation of electrophysiological changes

The motor evoked potential (MEP) was measured in each rat as described previously (Chen et al., 2017) 8 weeks after the SCI. Briefly, the rats were anesthetized by intraperitoneal injection of 5% chloral hydrate (7 mL/kg). Stimulating electrodes were placed at the intersection of the coronal and sagittal sutures. The recording electrode was placed over the posterior tibial nerve. The stimulation intensity was 46 V, the stimulation frequency was 1 Hz, the stimulation pulse width

was 0.2 ms, and the volatility was 540 μV. The MEP signals of the left and right hind limbs were recorded using Nicolet Viking Quest evoked potential equipment (Nicolet Biomedical Inc., San Carlos, CA, USA).

MEP recording was performed in canines 6 months after the SCI using the same recording equipment to evaluate the recovery of motor function (Jiang et al., 2018). Four stimulating electrodes were inserted into the biceps femoris of the left and right hind limbs and the cranial muscles corresponding to the human C1 and C2 regions according to the standard 10–20 international electrode placement system. Stimulation was applied with a voltage of 80–160 V (pulse width of 0.5 ms and stimulation frequency of 150 Hz).

Magnetic resonance imaging
At 6 months after surgery, a 3.0 T magnetic resonance imaging (MRI) scanner (Magnetom Verio, Siemens, Germany) was used to visualize the recovery of the SCI site in each canine. The T2-weighted image (T2WI) data were obtained with a repetition time of 3200 ms and an echo time of 77 ms at a layer thickness of 1.5 mm in a 256 × 256 scan, matrix with a field of view of 80 mm × 64 mm. Data were acquired five times.

Clinical experiment
Patients
A phase I open-label clinical trial was approved by the Ethics Committee of the Characteristic Medical Center of Chinese People's Armed Police Force on February 3, 2016 (approval No. PJHEC-2016-A8). This trial was conducted in accordance with the *Declaration of Helsinki* and registered at ClinicalTrials.gov as NCT 02510365 in February 2016. All patients provided written informed consent.

Forty patients with acute complete cervical SCI were selected at the Characteristic Medical Center of Chinese People's Armed Police Force. Before enrollment, 32 of the patients underwent posterior decompression and stabilization, and the remaining 8 patients received the same therapy with an anterior approach.

Forty patients were divided into the treatment group (*n* = 20) and control group (*n* = 20). In the treatment group, a hUC-MSC-laden CS was implanted in the injury site of each patient. The control group did not receive the transplant. There was no significant difference in the sex distributions, ages, American Spinal Injury Association (ASIA) Impairment Scale scores, activities of daily living (ADL) scores, residual urine volumes, or lesion lengths before enrollment between the two groups ($P > 0.05$; **Tables 1** and **2**). **Table 2**

Table 1 Patient characteristics between the two groups at baseline

Items	Treatment group	Control group	*P* value
Age (yr)	33.70±9.03	34.55±10.89	> 0.05
Sex (male/female)	5/15	7/13	> 0.05
Time after injury (d)	12.45±5.74	13.10±5.23	> 0.05
RUV (mL)	218.75±55.00	212.50±44.56	> 0.05
Motor score	18.45±4.34	17.65±4.51	> 0.05
Sensory score	30.95±5.04	32.30±5.38	> 0.05
ADL score	22.00±6.57	24.00±7.36	> 0.05

Data are expressed as the mean ± SD or *n*. ADL: Activities of daily living; RUV: residual urine volume; Motor and seneory functions were assessed using the ASIA motor and sensory scores.

Table 2 Mechanisms of the injury and the initial magnetic resonance imaging characteristics of all patients

Patient	Mode	Mechanism	Lesion length (cm)	Patient	Mode	Mechanism	Lesion length (cm)
Treatment group				*Control group*			
1	FFH	Fracture dislocation	1.5	1	FFH	Fracture dislocation	2.2
2	FFH	Compression	2.5	2	FFH	Fracture dislocation	1.2
3	FFH	Compression	3.1	3	TA	Burst fracture	1.5
4	TA	Flexion distraction	2.7	4	FFH	Compression	3.2
5	TA	Burst fracture	1.1	5	TA	Burst fracture	4.0
6	TA	Fracture dislocation	3.3	6	TA	Fracture dislocation	2.8
7	FFH	Compression	3.9	7	TA	Fracture dislocation	3.4
8	TA	Burst fracture	0.8	8	FFH	Flexion distraction	2.3
9	TA	Fracture dislocation	0.7	9	FFH	Burst fracture	0.7
10	TA	Fracture dislocation	2.1	10	TA	Fracture dislocation	3.5
11	TA	Burst fracture	1.8	11	FFH	Compression	1.3
12	FFH	Burst fracture	0.9	12	TA	Fracture dislocation	1.8
13	FFH	Flexion distraction	2.3	13	TA	Fracture dislocation	1.1
14	TA	Fracture dislocation	0.6	14	TA	Fracture dislocation	2.7
15	TA	Burst fracture	3.8	15	TA	Flexion distraction	1.6
16	TA	Flexion distraction	3.2	16	TA	Burst fracture	1.0
17	FFH	Burst fracture	1.4	17	TA	Burst fracture	2.4
18	FFH	Fracture dislocation	1.7	18	FFH	Flexion distraction	0.9
19	TA	Fracture dislocation	1.3	19	FFH	Fracture dislocation	3.3
20	TA	Flexion distraction	2.6	20	FFH	Compression	1.9

FFH: Fall from height; TA: traffic accident.

shows the mechanisms of the injuries and the initial MRI characteristics of all patients before treatment.

Inclusion criteria

All patients were (1) male or female adults (18–65 years old) (2) diagnosed as having acute complete cervical SCI according to the ASIA Impairment Scale, MRI, and electrophysiology (Xiao et al., 2018) and (3) the ASIA Impairment Scale (4) from the 4th cervical (C4) to the 7th cervical (C7) vertebrae (5) occurring within past 21 days. In addition, all study participants (6) were willing and able to make regular visits to the study site for treatment and follow-up according to the study protocol.

Exclusion criteria

(1) Patients who participated in another trial before enrollment and those exhibiting (2) serious complications were excluded from the study. In addition, patients who were (3) lactating or pregnant, (4) had a history of immune-mediated reactions or serious allergies, (5) had primary hematologic disorders, (6) had alcohol drug abuse/dependence, (7) took any drug or treatment known to cause major organ system toxicity during the past four weeks, or (8) had any other condition that might increase the risk to the subject or interfere with the clinical trial were also excluded.

Surgical procedure and implantation of hUC-MSC-laden CS

The control group received conventional treatment, such as infection prevention and supportive treatment. The patients in the treatment group received the CS with hUC-MSCs in addition to the conventional treatment. After induction of general anesthesia, the patient was placed on the operating table. A pre-incisional antibiotic (2 g ceftriaxone) was administered intravenously. The surgical level was determined based on the pre-operative MRI and computed tomography (CT) images. The intraoperative site was localized using a lateral spine X-ray. A posterior midline incision was marked and sterilized at the level of injury. After the musculature was separated from the spinous process, a laminectomy was performed at the same level using a bone rongeur. Under an operating microscope, the injured dura was incised and suspended to both sides to expose the spinal cord. The injured spinal cord mainly consisted of necrotic tissue (**Figure 2A**). Intraoperative neuroelectrophysiological measurements, somatosensory-evoked potentials (SSEP) and MEP, were taken to locate the rostral and caudal boundaries of the necrotic tissue, (Xiao et al., 2016). To locate the rostral necrotic tissue, electromyography stimulating electrodes (XLTEK®; Natus®, Oakville, Ontario, Canada) were positioned near the rostral end of the SCI site, and recording electrodes were placed on the scalp. If a normal SSEP response was detected, the position of the stimulating electrodes was deemed as normal spinal cord tissue; if no SSEP response was detected, the position of the stimulating electrodes was considered to be necrotic tissue. To locate the caudal necrotic tissue, the stimulating electrodes were positioned near the caudal end

of the SCI site, and the recording electrodes were placed on the sphincter ani externus. If a normal MEP response was detected, the position of the stimulating electrodes was considered to be normal spinal cord tissue; if no MEP response was detected, the position of the stimulating electrodes was deemed as necrotic tissue. Then, the necrotic tissue between the two identified boundaries was carefully removed under the operating microscope. The length of the gap in the spinal cord was measured. 4×10^7 hUC-MSCs were loaded in an approximately 10 mm-diameter bundle of CS, which was trimmed to the length of the gap and transplanted into the SCI site to fill the defect (**Figure 2B**). The dura was tightly sutured and repaired (**Figure 2C**). The spine was stabilized by internal fixation with a titanic alloy pedicle screw (Medtronic, Minneapolis, MN, USA; **Figure 2D**). The muscles, fascia, and subcutaneous tissue were then sutured sequentially. All surgeries were performed by an experienced neurosurgeon.

Rehabilitation program

All patients in the treatment and control groups underwent constant and regular rehabilitation for 6 months following surgery. The important components of rehabilitation programs included respiration, urination, muscle strength, joint motion, movement, wheelchair use, gait, and ADL.

Neurophysiologic studies

Nicolet Viking Quest evoked potential equipment (Nicolet Biomedical Inc.) was used to conduct neurophysiologic examinations before the surgery and 12 months after the surgery. The MEP and SSEP were measured to evaluate the recovery of motor and sensory functions. MEP measurements were taken with scalp stimulation to assess the muscle response as follows. Stimulating electrodes were placed on the scalp (on the frontal and parietal areas and on the vertex), and recording electrodes were positioned on the target muscles (on the upper and lower limbs, respectively). A single-pulse stimulus was applied to evoke an electrical response. The SSEP was performed by stimulating the median or posterior tibial nerves and measuring the response in the upper or lower limbs, respectively, as follows. To evaluate the upper limb response, the stimulating electrodes were positioned on the wrist to stimulate the median nerve, and the recording electrodes were placed on the contralateral C3'/C4'. To evaluate the lower limb response, the stimulating electrodes were positioned on the ankle, and the recording electrodes were placed at the contralateral Cz'. All electrophysiological measurements were conducted by the same neurologist.

Magnetic resonance imaging

Prior to surgery (baseline), and 12 months after surgery, a 3.0 T MRI scanner (MAgnetom Verio) was used to image each participant. The T2WI data were recorded with a repetition time of 3000 ms and an echo time of 90 ms at a layer thickness of 3.5 mm in a 269 × 384 scan matrix with a field of view of 272 cm × 275 cm. In addition, a workstation (Advantage Windows, version 4.2; GE Healthcare, Waukesha,

WI, USA) was used to capture diffusion tensor imaging (DTI) images with a repetition time of 6100 ms and echo time of 73 ms at a layer thickness of 1.5 mm in a 96 × 96 scan matrix with a field of view of 107 mm × 107 mm; the b-value was 600 s/mm^2. The image acquisitions were repeated six times. The apparent diffusion coefficient (ADC) and fractional anisotropy (FA) values of the spinal cord segments were determined using FuncTool software (GE Healthcare). All MRIs were performed by the same radiologist, and the images were captured by a second radiologist.

Neurological function assessment
Neurological function was assessed in terms of the ASIA motor and sensory scores, ADL score (Dai et al., 2013), and bowel and bladder function before transplantation and 12 months after transplantation. The maximum ASIA motor score is 100, the maximum sensory score is 224, and the maximum ADL score is 100; on all scales, higher scores indicate better patient recovery. The residual urine volume was measured using a B-mode ultrasound system (GE Healthcare) and calculated as 0.5 × top-to-bottom diameter × left-to-right diameter × anteroposterior diameter. All ultrasound images were captured by the same sonographer and assessed by the same neurologist to eliminate inter-rater variability.

Postoperative follow-up
The follow-up time was 12 months after surgery for both the treatment and control groups.

Statistical analysis
Data are presented as the mean ± standard deviation (SD). Data were analyzed using the SPSS 15.0 package (SPSS, Chicago, IL, USA). Statistically significant differences in age, time of injury, ASIA scores, ADL scores, residual urine volume, lesion length, ADC, fractional anisotropy (FA), and OD value were determined by a two-sample *t*-test and paired *t*-test. A Chi-square test was used to compare classification variables, such as sex. One-way analysis of variance followed by the Student-Newman-Keul *post hoc* test was used to compare BBB scores, Rivlin slope scores, Olby scores, and MEP measurements in the preclinical experiments. *P* values less than 0.05 were considered statistically significant.

Results
Pre-clinical studies
Structure and biocompatibility of the CS
The CS was freeze-dried for visual analysis (**Figure 3A**). Scanning electron microscopy images showed that the CS had a three-dimensional porous structure and that the pores were interconnected (**Figure 3B** and **C**). Phase-contrast microscopy images after 3 days of incubation with hUC-MSCs revealed that the cells were mostly fusiform or flat (**Figure 3D**). Immunofluorescence staining at this time point revealed that the hUC-MSCs expressed typical MSC markers, CD105, CD73, and CD90 (**Figure 3E–H**), as well as specific hUC-MSC biomarkers, CD73, CD90, and CD105 (**Figure 3I–L**). After the CSs were incubated with the hUC-MSCs for

7 days, inverted phase-contrast microscopy and scanning electron microscopy images showed that the hUC-MSCs adhered firmly to the surface of the CS and were growing well inside the pores (**Figure 3M** and **N**).

The proliferation of hUC-MSCs in the CS and control groups over 7 days was evaluated using the Cell Counting Kit 8 (CCK-8) assay. There was no statistically significant difference between the OD values of the two groups at any time point (*P* > 0.05; **Figure 3O**), indicating that the CS had good cytocompatibility.

Implanting the hUC-MSC-laden CS improves locomotor function after SCI in rats and canines
Recovery of motor function in rats: Before surgery, the BBB scores were 21 points for all groups. Immediately after the SCI, the hindlimbs of rats were completely paralyzed. In the two weeks following injury, the BBB scores of the SCI, CS, and CS + hUC-MSCs groups were below 3 points. However, 4, 6, and 8 weeks after injury, the BBB scores in the CS + hUC-MSCs group were significantly higher than those in the SCI and CS groups (*P* < 0.05; **Figure 4A**).

In the modified Rivlin slope experiment, 3, 4, 6, 8 weeks after injury, the highest inclination angles in the CS + hUC-MSCs and CS groups were significantly larger than those in the SCI group (*P* < 0.05; **Figure 4B**). Furthermore, the angle in the CS + hUC-MSCs group was significantly higher than that in the CS group at 3, 4, 6, and 8 weeks after injury (*P* < 0.05; **Figure 4B**). In the SCI group, the rats passively dragged their hind limbs, and their hind paws often fell off the grid; they struggled to climb the inclined mesh with their forelimbs (**Figure 3C**). However, the rats in the CS and CS + hUC-MSCs groups could place their paws on each level of the grid and kept their hind limbs on the grid (**Figure 4D** and **E**). Moreover, in the CS + hUC-MSCs group, the rats' hind limbs were more powerful, their front and rear limbs were more coordinated, and they made more attempts to move their hind limbs onto the grid compared with the CS group.

To evaluate axonal regeneration, an electrophysiological examination was performed at 8 weeks after the injury. The amplitude and latency were notably improved in the CS + hUC-MSCs group and CS group compared with the SCI group (**Figure 5A–C**). The results showed that implantation of the hUC-MSC-laden CS markedly enhanced the amplitude and shortened the latency of MEPs compared with implantation of the CS without hUC-MSCs (**Figure 5A–C**).

Recovery of motor function in canines: The Olby scoring scale was performed to assess the locomotion recovery int he canines after surgery. The Olby scores in the SCI, CS, and CS + hUC-MSCs groups were below 2 points within the first month after surgery but gradually increased in the following months, indicating gradual recovery of motor function (**Figure 4F**). At 3, 4, 5, and 6 months after injury, the Olby scores in the CS group and the CS + hUC-MSCs group were significantly greater than those in the SCI group (*P* < 0.05 and *P* < 0.01, respectively; **Figure 4F**). Furthermore, during the period of 3–6 months after injury, the Olby scores in the CS + hUC-MSCs group were significantly better than those

in the CS group ($P < 0.05$; **Figure 4F**). After 6 months of recovery after injury, the hind limbs of the canines in the CS + hUC-MSCs and CS groups showed some standing and ambulating abilities, while the SCI group demonstrated no voluntary movement (**Figure 4G–I**). In addition, the amplitude and latency of the MEP were noticeably improved in the CS + hUC-MSCs group compared with the CS and SCI groups (**Figure 5D–F**). These results indicate that the implantation of the hUC-MSC-laden CS can improve muscle strength and result in more frequent weight-bearing behavior during movement compared with no treatment or implantation of the CS alone.

Implanting the hUC-MSC-laden CS facilitates nerve fiber regeneration after SCI in canines

At 6 months after surgery, T2WI of the CS + hUC-MSCs group showed continuity between the rostral and caudal stumps of the transected spinal cord. In addition, more regenerated nerve fibers traversing the lesion gap were observed in the CS and CS + hUC-MSCs groups than in the SCI group (**Figure 6B1**, **B2**, **C1**, **C2**, **D1**, and **D2**). Furthermore, CS + hUC-MSCs group exhibited markedly better regeneration of nerve fibers at the injury site than the CS group (**Figure 6C1**, **C2**, **D1**, and **D2**).

Clinical trial
Implanting the hUC-MSC-laden CS improves neurological function after SCI in humans

ASIA grade change: In the treatment group, nine patients (45%) improved from ASIA grade A to B, and two (10%) improved from grade A to C. In the control group, no improvement was recorded in terms of ASIA grading.

ADL score improvement: To confirm the recovery of neurological function, the ADL score was assessed. Results showed that one patient recovered flexion and extension of the left little finger 12 months after treatment. The motor, and ADL scores before and after transplantation were significantly different in the treatment group ($P < 0.05$) but not in the control group ($P > 0.05$; **Table 3**).

Implanting the hUC-MSC-laden CS facilitates bowel and bladder function recovery after SCI in humans

In the treatment group, the residual urine volume at 12 months (139.20 ± 42.20 mL) was significantly decreased compared with preoperative residual urine volume (218.75 ± 55.00 mL; $P < 0.05$). However, the residual urine volume in the control group was not significantly different before

and after recruitment (212.50 ± 44.56 and 203.60 ± 43.44 mL, respectively; $P > 0.05$). In the treatment group, two patients (10%) partially recovered urination and defecation after 12 months. On the contrary, bowel and bladder functions were not significantly altered in the control group during follow-up.

Electrophysiological findings

MEP improvement: In the treatment group, two patients (10.0%) exhibited no MEP signal before treatment (**Figure 7A**) but significant MEP in the lower limbs 12 months after the treatment (**Figure 7B**). Of the patients who exhibited some MEP activity before treatment, nine (45.0%) demonstrated improvements in the MEP latency and amplitude while the other nine (45.0%) did not exhibit any change. In the control group, no patients showed improvement in the MEP activity.

SSEP improvement: In the treatment group, the SSEP latency and amplitude in the lower limbs were significantly improved in two patients (20.0%) after 12 months compared with the pre-operative measurements (**Figure 7C** and **D**). None of the patients in the control group showed improvement in terms of the SSEP activity.

Magnetic resonance imaging and diffusion tensor imaging findings

In the treatment group, T2WI showed that there was a cavity at the spinal cord before treatment. However, after 12 months of recovery following treatment, this cavity disappeared, and nerve-fiber-like streaks appeared while the diameter of the spinal cord slightly increased where the hUC-MSC-laden CS was implanted (**Figure 8B1**, **B2**, **B5**, and **B6**). Compared with the preoperative DTI, the DTI at 12 months following treatment confirmed that continuous fibers were newly formed during recovery (**Figure 8B3**, **B4**, **B7**, and **B8**). There was no evidence of tumorigenesis at the implant site. In the control group, the T2WI before and after enrollment showed that the cavity at the injury site did not noticeably change, and the DTI did not reveal any continuous fiber signaling (**Figure 8A1–A8**). In the treatment group, the FA values were notably higher ($P < 0.01$), and the ADC values were significantly lower than in the control group ($P < 0.01$; **Figure 8C** and **D**).

Adverse events

All adverse events in the treatment group during follow-up were recorded (**Table 4**). No serious adverse events asso-

Table 3 Comparison of motor, sensory and ADL scores in patients between both groups

| Items	Treatment group		Control group	
	Before transplantation	After transplantation	Before observation	After observation
Motor score	18.45±4.34	27.6±5.48[†]	17.65±4.51	18.39±4.43
Sensory score	30.95±5.04	40.85±6.24[†]	32.30±5.38	32.95±5.17
ADL score	22.00±6.57	32.50±10.94[†]	24.00±7.36	26.25±6.46

Data are expressed as the mean ± SD (paired *t*-test). [†]$P < 0.05$, *vs.* before transplantation in treatment group; ADL: Activities of daily living. Motor and seneory functions were assessed using the ASIA motor and sensory scores.
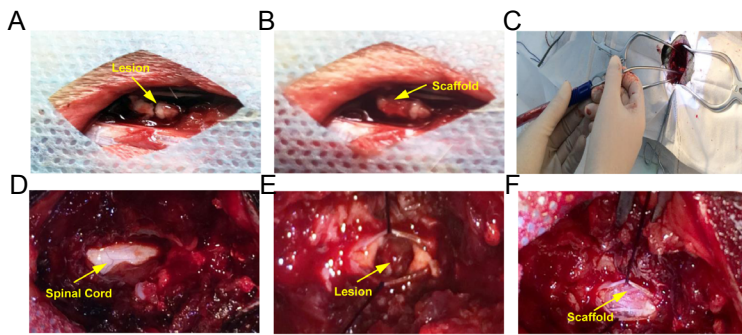
Figure 1 Spinal cord transection in rats (A, B) and canines (C–F).
(A) Transection of the spinal cord (yellow arrow). (B) Implantation of the CS (yellow arrow). (C) SCI model was established under an operating microscope. (D) Exposure of the spinal cord (yellow arrow). (E) Transection of the spinal cord (yellow arrow). (F) Implantation of the CS (yellow arrow). CS: Collagen scaffold; SCI: spinal cord injury.
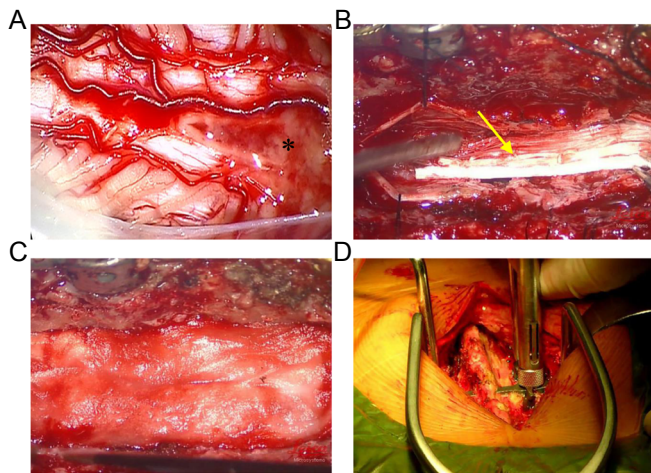

Figure 2 Necrotic tissue resection and collagen scaffold implantation in the treatment group.
(A) The spinal cord was exposed after opening the dura mater; the asterisk denotes necrotic tissue. (B) Collagen scaffold with human umbilical cord-mesenchymal stem cells (yellow arrow) transplanted into the gap in the spinal cord. (C) The damaged dura mater was repaired by implanting an artificial dura mater to prevent cerebrospinal fluid leakage. (D) A metallic material was used to repair the spine.
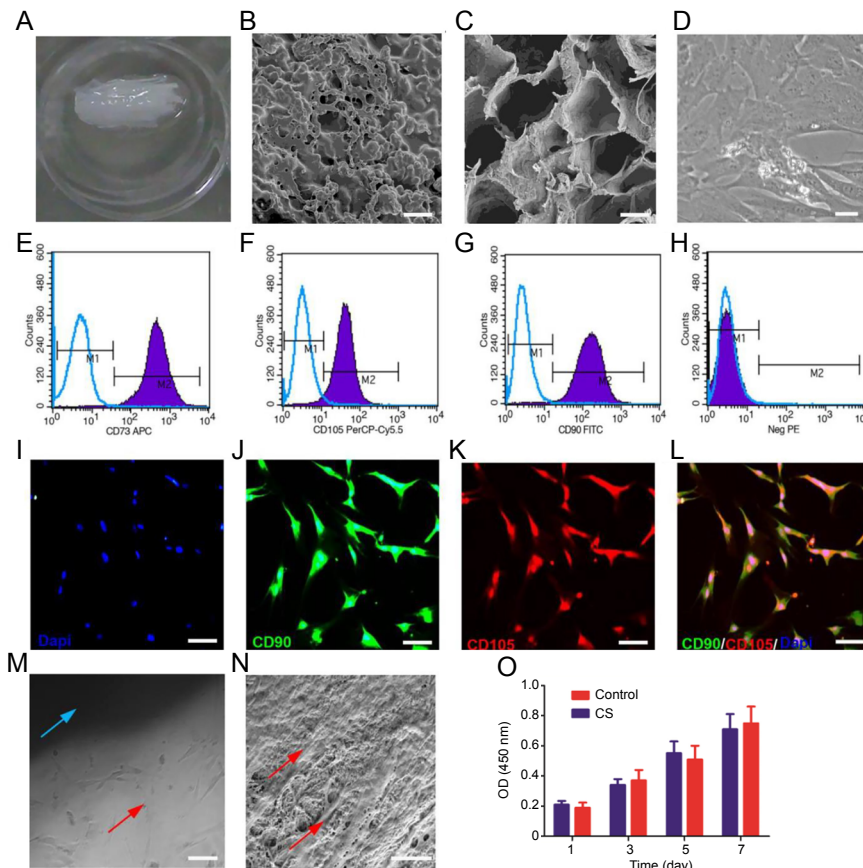

Figure 3 Morphology and characterization of human umbilical cord-mesenchymal stem cells (hUC-MSCs) and the collagen scaffold (CS).
(A) CS. (B, C) Scanning electron microscope images of the CS. (D) hUC-MSC morphology observed by phase-contrast microscopy. (E–H) Flow cytometry analysis of cell surface markers with antibodies against CD73, CD90, and CD105. (I–L) Immunofluorescence images of hUC-MSCs immunostained with CD73, CD90, and CD105: blue indicates DAPI, green indicates CD90, and red indicates CD105. (M) Morphological observation of hUC-MSCs cultured on the CS under a phase-contrast microscope: the blue arrow denotes the CS, and the red arrow denotes hUC-MSCs. (N) Morphology of the CS co-cultured with hUC-MSCs as visualized by scanning electron microscopy: the red arrows indicate hUC-MSCs. (O) Cell Counting Kit-8 assay of the hUC-MSCs cultured with the CS after 1, 3, 5, and 7 days of co-culture. Data were expressed as the mean ± SD. Scale bars: 5 μm in B, N; 10 μm in C; 100 μm in D, I, J, K, L; 200 μm in M. CD: Cluster of differentiation; CD73APC: cluster of differentiation 73 antigen-presenting cell; DAPI: 4,6-diamino-2-phenyl indole; FITC: fluorescein isothiocyanate; NegPE: negative phycoerythrin; OD: optical density; PerCP-Cy5.5: polydinoflavin-chlorophyll-protein complex-Cyanine 5.5.
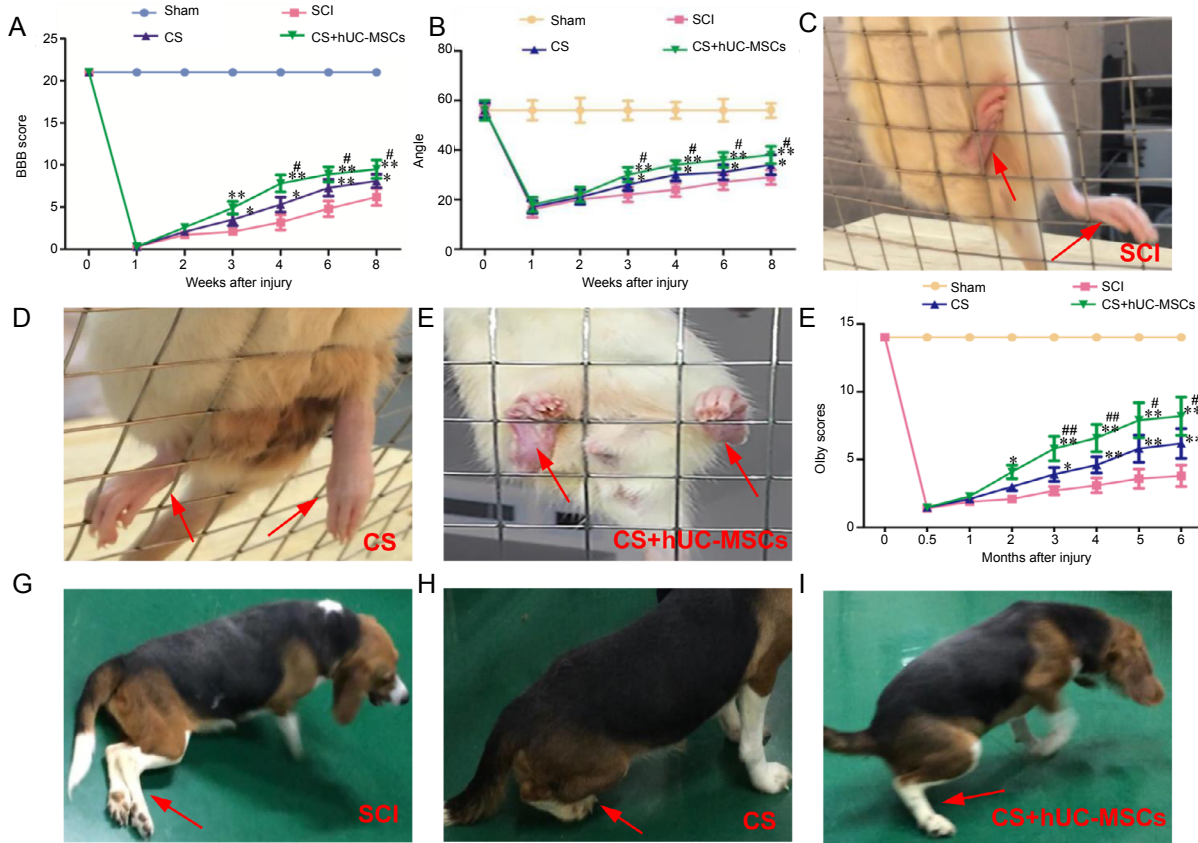
Figure 4 Post-injury behavioral evaluations in rats (A–E) and canines (F–I).
(A) BBB scores before and 1, 2, 3, 4, 6, and 8 weeks after surgery (*n* = 10). (B) Modified Rivlin slope experiment results before and 1, 2, 3, 4, 6, and 8 weeks after surgery (*n* = 10). (C–E) Representative images of rats in the SCI group (C), the CS group (D), and the CS + hUC-MSCs group (E) during the slope grid experiment at 8 weeks post-injury. (F) Olby scores before and 0.5, 1, 2, 3, 4, 5, and 6 months after surgery (*n* = 5). (G–I) Representative images of canines in the SCI group (G), the CS group (H), and the CS + hUC-MSCs group (I) during the slope grid experiment at 6 months post-injury. The red arrows indicate the hind limbs. Data are expressed as the mean ± SD (one-way analysis of variance followed by the Student-Newman-Keul *post hoc* test). ∗*P* < 0.05, ∗∗*P* < 0.01, *vs.* SCI group; #*P* < 0.05, ##*P* < 0.01, *vs.* CS group. BBB: Basso-Beattie-Bresnahan; CS: collagen scaffold; hUC-MSCs: human umbilical cord-mesenchymal stem cells; SCI: spinal cord injury.
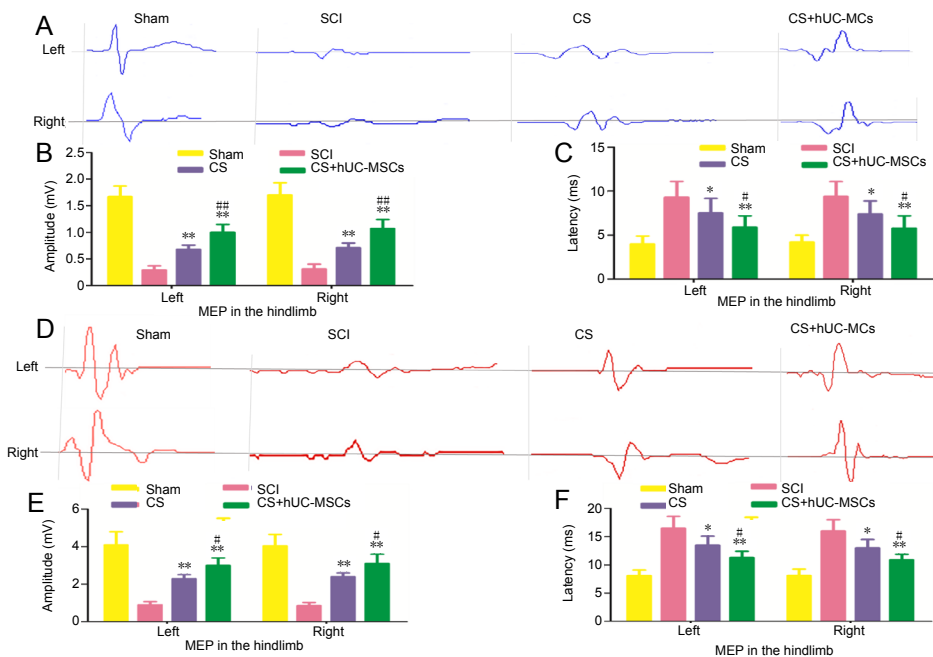
Figure 5 Electrophysiological results for all groups.
(A) MEP traces of the left and right hindlimbs of rats at 8 weeks after surgery. (B, C) Amplitude (B) and latency (C) of the MEPs in the left and right hindlimbs of rats at 8 weeks after surgery (*n* = 10). (D) MEP traces of the left and right hindlimbs of canines at 6 months after surgery. (E, F) Amplitude (E) and latency (F) of the MEPs in the left and right hindlimbs of canines at 6 months after surgery (*n* = 5). Data are expressed as the mean ± SD (one-way analysis of variance followed by the Student-Newman-Keul *post hoc* test). ∗*P* < 0.05, ∗∗*P* < 0.01 *vs.* SCI group; #*P* < 0.05, ##*P* < 0.01, *vs.* CS group. CS: Collagen scaffold; hUC-MSCs: human umbilical cord-mesenchymal stem cells; MEP: motor evoked potential; SCI: spinal cord injury.

Table 4 Adverse events in the treatment group

Adverse events	*n*(%)	Corresponding treating measures
Intracranial infection	–	No complications
Cerebrospinal fluid leakage	–	No complications
Tumorigenesis	–	No complications
Neurologic deterioration	–	No complications
Constipation	6(30)	Symptomatic treatment
Urinary system infection	5(25)	Antibiotic injection
Pulmonary infection	4(20)	Antibiotic injection
Psychological disorder	4(20)	Psychological intervention
Osteoporosis	3(15)	Medication therapy (alendronate sodium, calcium)
Pressure sores	2(10)	Strengthening nursing, dressing change daily
Deep venous thrombosis	1(5)	Anticoagulation and thrombolysis therapy

ciated with the transplantation, such as cerebrospinal fluid leakage, tumorigenesis, neurologic deterioration, or intracranial infection, were observed. A minority of the patients exhibited mild adverse events: Six patients (30%) reported constipation, which was mitigated by symptomatic treatment. Five patients (25%) developed urinary system infections. Four patients (20%) suffered from psychological disorders, but these conditions were resolved by psychological intervention. Four patients (20%) suffered from pulmonary infections, which were cured with antibiotics. Three patients (15%) had osteoporosis, which was addressed by prescribing medication. Two patients (10%) developed pressure sores, which were healed by providing additional nursing care and changing the wound dressing daily. One patient (5%) underwent deep venous thrombosis 2 months after the operation, and after this the patient was cured by anticoagulation and thrombolysis therapy.

Discussion

SCI leads to the disruption of axons, resulting in severe deficits of motor and sensory functions below the level of injury as well as urination and defecation (Dyck and Karimi-Abdolrezaee, 2018). Conventional therapeutic methods, including operation, pharmacology, and rehabilitation, have no robust effects on neurological repair. Functional electrical stimulation merely improves some of the effects associated with SCI such as spasticity, neuropathic pain, and disturbances in urination and defecation functions (Ahuja et al., 2017). There is still no effective therapy to improve motor and sensory functions following SCI.

MSCs can not only differentiate into neural tissue, such as neurons, astrocytes, and oligodendrocytes, but can also produce immunoregulatory cytokines, inhibit astrogliosis and microglial activation, and secrete growth factors (Cízková et al., 2006; Ruff et al., 2012; Ritfeld et al., 2015; Noh et al., 2016). Biomaterials previously applied in clinical studies were mainly neural tubes comprising polylactic acid and glycolic acid (Theodore et al., 2016) and CSs (Zhao et al., 2017; Xiao et al., 2018). CSs have been shown to bridge the gap of the

lesion and form a suitable microenvironment at the injury site, guiding and providing support for axon growth along its fibers and inhibiting scar formation in rat and canine models. CSs also act as carriers to better deliver nerve growth factor to stem cells to promote neural regeneration (Han et al., 2009, 2010, 2015; Orive et al., 2009; Li et al., 2013; Führmann et al., 2017). Hence, it is expected that CSs loaded with stem cells will be a new strategy for SCI treatment.

The preclinical results with rat models confirmed that the CS can reduce the lesion area, guide the orderly regeneration of nerve fibers, and promote recovery of neurological function. Subsequently, the same results were seen in canine models.

Several clinical trials have been done to evaluate the safety of transplanted human cells of different origin in patients with acute or chronic SCI. First, the transplantation of Schwann cells and olfactory ensheathing cells into injured spinal cords was shown to promote axonal regeneration and myelination. The study demonstrated that this method was safe and feasible, but no obvious effect on patients with SCI was found (Féron et al., 2005; Anderson et al., 2017). Second, Curtis et al. (2018) grafted fetal spinal cord-derived neural stem cells in four patients with chronic SCI (T2–12, pre-operative ASIA grade A) 12–24 months after injury. Their results indicated that the treatment was well tolerated in all patients for 18–27 months after grafting. However, motor, sensory, and electrophysiological results showed that only 2 of the 4 patients exhibited mild changes at 1 or 2 neurological levels. In our study, neurological function significantly improved in transplanted patients. Third, a recent phase III clinical trial of mesenchymal stem cell transplantation demonstrated patient safety, but the expected recovery of motor function was not observed (Oh et al., 2016). Although these studies did not achieve satisfactory therapeutic effects, no complications were observed. Overall, these clinical trials have demonstrated the safety and feasibility of stem cell grafting in patients with acute or chronic SCI. However, until now, grafting of hUC-MCs on a CS has not been tested in clinical studies for the treatment of SCI. CS is a well-known biomaterial for nerve regeneration and is authorized by the China Food and Drug Administration for experimental spinal transplantation in patients. The results of our clinical trial supported our findings in animal models, indicating that this technique is safe and effective for patients with complete SCI.

From a safety perspective, no surgery related to severe adverse events, such as intracranial infection or cerebrospinal fluid leakage, was noted in any of the patients. There were several mild adverse events, including urinary system infection, psychological disorder, constipation, deep venous thrombosis, and pressure sores. However, these events are common symptoms associated with SCI, and it is unlikely that they were related to the transplantation of hUC-MSC-laden CS. In addition, the motor, sensation, and residual urine volume data showed that no patient underwent neurologic deterioration over the 12 months post-transplantation. Further, MRI analysis showed no detectable hemorrhage, inflammatory change, syringomyelia, or tumorigenesis in or

around the transplantation area in any of the patients. We have performed a 12-month follow-up, but longer-term follow-up is important to fully assess possible complications.

Compared with the baseline, the scores of motor, sensation, and ADL were significantly enhanced in the treatment group; however, no improvement was observed in any patients in the control group. The increases in ADL scores reflected improved ability to carry out daily activities such as dressing and moving, which reflects improved motor function. In the treatment group, 45% of patients were re-diagnosed from a "complete" SCI to an "incomplete" SCI in the 12 months following treatment. The ADL scores and ASIA grades also demonstrated that the implantation of the hUC-MSC-laden CS facilitated better recovery of neural function in patients with SCI compared with the control group. The electrophysiological results further supported the finding that this treatment improved motor and sensory functions after SCI. The improvement in the MEP response may be attributed to the establishment of new reticular circuitry and functional reconnection of spinal motor centers. Even though axon regeneration may have begun during the study period, the velocity of the axonal growth in the central nervous system may be slower than the elongation rate of peripheral nerves, which is approximately 0.25 mm per day through scar tissue (Xiao et al., 2016). Therefore, a long-term clinical follow-up is merited, and the data are expected to be intriguing.

The improvement of motor and sensory functions is considered as a primary result to assess therapeutic effects in SCI. However, the function of the bowel and bladder has important clinical consequences and is indispensable in the evaluation of neurological recovery. Urination and defecation dysfunction in patients with SCI are common clinical manifestations that respond poorly to conventional treatment; there are no effective therapeutic methods to recover urination and defecation function. In the treatment group in our clinical study, the residual urine volume post-transplantation significantly decreased compared with the baseline; in contrast, the residual urine volume in the control group did not change significantly. Similarly, Dai et al. (2013) reported a mild improvement in residual urine volume after treatment with bone marrow mononuclear cells (BMSCs) in patients with SCI. In addition, partial defecation reflex was restored in two patients in our treatment group. This improvement in urination and defecation functions was an inspiring result because it is a very important aspect of neurological recovery.

Previous studies have reported changes under MRI after stem cell therapy in SCI (Park et al., 2012). The MRI results in the treatment group showed neurological recovery, including the appearance of fiber-like streaks in the cavity, increased cord diameter at the injury site, and a decreased cavity size. However, the MRI results of the control group showed no changes. To describe results of 10 patients who underwent after MSC therapy for SCI, Park et al. (2012) reported MRI observations that were similar to our results. However, there was no significant linear correlation between MRI changes and neural function improvement (Oh et al.,

2016). Furthermore, based on conventional MRI sequences, the fiber-like steaks observed at the injury site may not be specific to axonal regeneration (Oh et al., 2016). As such, DTI was used to remedy deficiencies associated with routine MRI. DTI can be used to quantitatively evaluate white matter tracts and has been shown to accurately predict neurological recovery in patients with SCI (Chang et al., 2010; Rajasekaran et al., 2012; Liu et al., 2019; Poplawski et al., 2019). Compared with the control group, the FA and ADC values in the treatment group were notably improved after transplantation. In the treatment group, fiber continuity was not observed on DTI imaging before transplantation, but DTI imaging after transplantation showed the remodeling of fiber continuity at the injury site. These results indicate that the implantation of the hUC-MSC-laden CS filled the gap at the injury site and promoted nervous tissue repair and axonal regeneration.
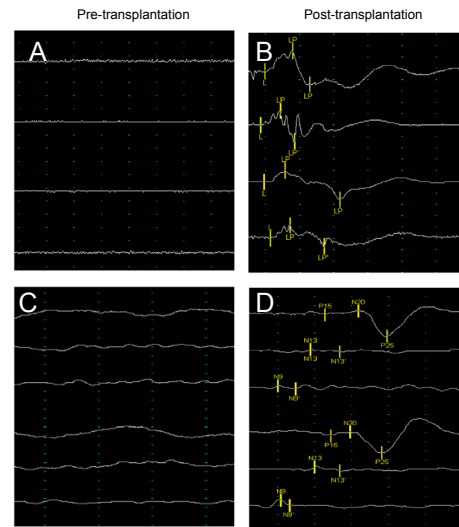
CSs can provide support and guidance for axonal regeneration, act as a carrier for cells at the injury site, and form a suitable microenvironment around the injury. In animal experiments, nerve fiber regeneration was shown to be significantly improved by implantation of a CS with hUC-MSCs. Similarly, studies have shown that CS combined with neural stem cells can guide the orderly regeneration of neural fibers, reduce diffusion of cells from the injury area, and promote the neuronal differentiation of transplanted stem cells or endogenous stem cells (Orive et al., 2009; Li et al., 2015; Führmann et al., 2017; Xu et al., 2017; Han et al., 2018). When hUC-MSCs were loaded on the CS, they adhered to the longitudinally arranged fibers, which prevented their diffusion from the injury site, and grew along the many tiny channels on the fibers. Furthermore, differentiated neurons can form neuronal relays throughout the lesion site, which may further reconstruct synaptic connections with host spinal cord neurons to transmit neural signals across the gap and promote functional restoration in SCI (Li et al., 2016, 2017b). We initially demonstrated that motor and sensory functions were markedly improved after the transplantation of hUC-MSC-laden CS in human patients. Analogous functional improvement patterns in animals and patients imply that this treatment may promote axonal regeneration in humans as observed in animals in previous studies.

Although exciting data were obtained in this study, the sample was limited; as such, the results should be confirmed in a multicenter study with long-term follow-up. Despite these shortcomings, the clinical results demonstrated the safety and efficiency of the hUC-MSC-laden CS and showed that the treatment may benefit patients by promoting the recovery of neural function.

Our clinical study demonstrated, for the first time, that the implantation of a hUC-MSC-laden CS is safe and effective in patients with SCI over a 12-month follow-up. Our preliminary results also demonstrate the feasibility of the therapy. In conjunction with the demonstrated potential efficacy in previous animal studies, these results indicate that this therapeutic strategy may lead to better recovery for SCI patients.
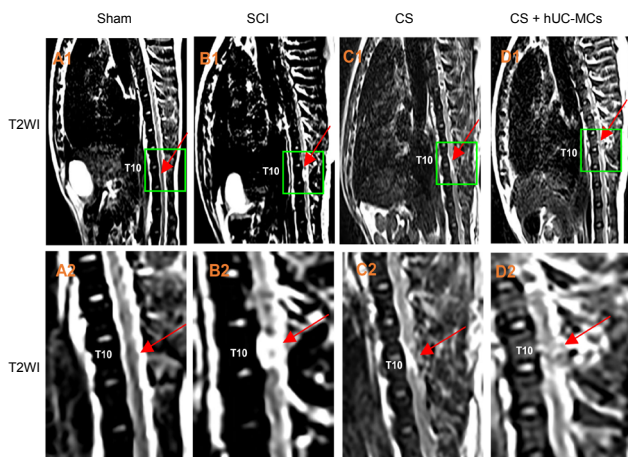
Figure 6 Magnetic resonance imaging of canines 6 months after surgery.

(A–D) T2WI images of the sham group (A1, A2), SCI group (B1, B2), CS group (C1, C2), and CS + hUC-MSCs group (D1, D2). (A2, B2, C2, D2) Magnified images of the regions delineated by the yellow boxes in A1, B1, C1, and D1, respectively. The red arrows denote segments involved in the SCI at T10. CS: Collagen scaffold; hUC-MSCs: human umbilical cord mesenchymal stem cells; SCI: spinal cord injury; T2WI: T2-weighted images; T10: tenth thoracic vertebrae.

Figure 7 Improvement in nerve electrophysiology in the treatment group after transplantation of the hUC-MSC-laden CS.

(A) No MEP wave was elicited in the patient before treatment. (B) The patient exhibited an obvious MEP wave 12 months after treatment. (C) No SSEP wave was elicited in the patient before treatment. (D) The latency and amplitude of the SSEP waves in the patient improved after treatment. The abscissa indicates latency, and the ordinate indicates amplitude. CS: Collagen scaffold; hUC-MSCs: human umbilical cord-mesenchymal stem cells; L: latency; MEP: motor evoked potential; N: nerve cortical; P: peripheral.

Figure 8 Typical T2-weighted images (T2WI) and diffusion tensor imaging (DTI).

(A1, A2) In the control group, the T2WI showed a cavity at C4 before treatment. (A5, A6) The sign of a cavity was still evident in the area of the SCI 12 months after treatment, and the discontinuity of the white matter fibers observed by preoperative DTI (A3 and A4, arrowhead) was still visibly by DTI 12 months after transplantation (arrowhead) (A7, A8, arrowhead). In the CS + hUC-MSCs group, the T2WI showed (B1, B2) a cavity at C6 before treatment and (B5 and B6) fiber-like streaks, the absence of a cavity, and an increased spinal cord diameter at the implantation site 12 months after treatment. In the CS + hUC-MSCs group, DTI showed discontinuity of the white matter fibers at C6 before treatment (B3, B4). The continuity of fiber signaling was newly observed at the injured cervical cord after transplantation (B7, B8). (C, D) Fractional anisotropy (FA) value and apparent diffusion coefficient (ADC) before transplantation and 12 months after transplantation. (A2, A4, A6, A8, B2, B4, B6, B8) Amplified images of the regions in the yellow boxes in A1, A3, A5, A7, B1, B3, B5, and B7, respectively. Red arrows indicate the spinal cord injury region. C4: The fourth cervical vertebra; C6: the sixth cervical vertebra. Data are expressed as the mean ± SD ($n = 5$; two-sample t-test). $\$\$P < 0.01$, $vs.$ control group.

Author contributions: *Study design: WSD, KM, BL; experiment implementation: WSD, XYL, HYX, JZ; data analysis: WSD, KM, HYX, HYS, HTS; material contribution and equipment coordination: SZ, XYC. All authors approved the final version of the paper.*

Conflicts of interest: *The authors declare that there are no conflicts of interest associated with this manuscript.*

Financial support: *This work was supported by the National Natural Science Foundation of China, No. 11932013 (to SZ), 11672332 (to SZ); the National Key Research and Development Plan of China, No. 2016YFC1101500 (to SZ); the Science and Technology Military-Civilian Integration Project of Tianjin of China, No. 18ZXJMTG00260 (to XYC); the Key Project of Science and Technology Support Plan of Tianjin of China, No. 17YFZCSY00620 (to XYC); the Rescue Medical Clinical Center Fund of Tianjin of China, No. 15ZXLCSY00040 (to XYC). The funding sources had no role in study conception and design, data analysis or interpretation, paper writing or deciding to submit this paper for publication.*

Institutional review board statement: *The clinical trial was approved by the Ethics Committee of the Characteristic Medical Center of Chinese People's Armed Police Force on February 3, 2016 (approval No. PJHEC-2016-A8). All animal experiments were performed in accordance with the Ethics Committee of the Characteristic Medical Center of Chinese People's Armed Police Force on May 20, 2015 (approval No. PJHEC-2015-D5).*

Declaration of patient consent: *The authors certify that they have obtained all appropriate patient consent forms. In the forms, the patients have given their consent for their images and other clinical information to be reported in the journal. The patients understand that their names and initials will not be published and due efforts will be made to conceal their identity, but anonymity cannot be guaranteed.*

Reporting statement: *The writing and editing of the article was performed in accordance with the Transparent Reporting of Evaluations with Nonrandomized Designs (TREND) statement.*

Biostatistics statement: *The statistical methods of this study were reviewed by the biostatistician of Gansu University of Chinese Medicine, China.*

Copyright license agreement: *The Copyright License Agreement has been signed by all authors before publication.*

Data sharing statement: *Datasets analyzed during the current study are available from the corresponding author on reasonable request.*

Plagiarism check: *Checked twice by iThenticate.*

Peer review: *Externally peer reviewed.*

Open access statement: *This is an open access journal, and articles are distributed under the terms of the Creative Commons Attribution-Non-Commercial-ShareAlike 4.0 License, which allows others to remix, tweak, and build upon the work non-commercially, as long as appropriate credit is given and the new creations are licensed under the identical terms.*

Open peer reviewer: *L Bauchet, CHU Montpellier, France.*

Additional file: *Open peer review report 1.*

References

Ahuja CS, Wilson JR, Nori S, Kotter M, Druschel C, Curt A, Fehlings MG (2017) Traumatic spinal cord injury. Nat Rev Dis Primers 3:17018.

Anderson KD, Guest JD, Dietrich WD, Bartlett Bunge M, Curiel R, Dididze M, Green BA, Khan A, Pearse DD, Saraf-Lavi E, Widerström-Noga E, Wood P, Levi AD (2017) Safety of autologous human Schwann cell transplantation in subacute thoracic spinal cord injury. J Neurotrauma 34:2950-2963.

Basso DM, Beattie MS, Bresnahan JC (1995) A sensitive and reliable locomotor rating scale for open field testing in rats. J Neurotrauma 12:1-21.

Brown AR, Martinez M (2019) From cortex to cord: motor circuit plasticity after spinal cord injury. Neural Regen Res 14:2054-2062.

Chang Y, Jung TD, Yoo DS, Hyun JK (2010) Diffusion tensor imaging and fiber tractography of patients with cervical spinal cord injury. J Neurotrauma 27:2033-2040.

Chen C, Zhao ML, Zhang RK, Lu G, Zhao CY, Fu F, Sun HT, Zhang S, Tu Y, Li XH (2017) Collagen/heparin sulfate scaffolds fabricated by a 3D bioprinter improved mechanical properties and neurological function after spinal cord injury in rats. J Biomed Mater Res A 105:1324-1332.

Cízková D, Rosocha J, Vanický I, Jergová S, Cízek M (2006) Transplants of human mesenchymal stem cells improve functional recovery after spinal cord injury in the rat. Cell Mol Neurobiol 26:1167-1180.

Curtis E, Martin JR, Gabel B, Sidhu N, Rzesiewicz TK, Mandeville R, Van Gorp S, Leerink M, Tadokoro T, Marsala S, Jamieson C, Marsala M, Ciacci JD (2018) A first-in-human, phase I study of neural stem cell transplantation for chronic spinal cord injury. Cell Stem Cell 22:941-950.

Dai G, Liu X, Zhang Z, Yang Z, Dai Y, Xu R (2013) Transplantation of autologous bone marrow mesenchymal stem cells in the treatment of complete and chronic cervical spinal cord injury. Brain Res 1533:73-79.

David S, Zarruk JG, Ghasemlou N (2012) Inflammatory pathways in spinal cord injury. Int Rev Neurobiol 106:127-152.

De Miguel MP, Fuentes-Julián S, Blázquez-Martínez A, Pascual CY, Aller MA, Arias J, Arnalich-Montiel F (2012) Immunosuppressive properties of mesenchymal stem cells: advances and applications. Curr Mol Med 12:574-591.

Dyck SM, Karimi-Abdolrezaee S (2018) Role of chondroitin sulfate proteoglycan signaling in regulating neuroinflammation following spinal cord injury. Neural Regen Res 13:2080-2082.

Fan J, Xiao Z, Zhang H, Chen B, Tang G, Hou X, Ding W, Wang B, Zhang P, Dai J, Xu R (2010) Linear ordered collagen scaffolds loaded with collagen-binding neurotrophin-3 promote axonal regeneration and partial functional recovery after complete spinal cord transection. J Neurotrauma 27:1671-1683.

Féron F, Perry C, Cochrane J, Licina P, Nowitzke A, Urquhart S, Geraghty T, Mackay-Sim A (2005) Autologous olfactory ensheathing cell transplantation in human spinal cord injury. Brain 128:2951-2960.

Fitch MT, Silver J (2008) CNS injury, glial scars, and inflammation: Inhibitory extracellular matrices and regeneration failure. Exp Neurol 209:294-301.

Führmann T, Anandakumaran PN, Shoichet MS (2017) Combinatorial therapies after spinal cord injury: how can biomaterials help. Adv Healthc Mater doi: 10.1002/adhm.201601130.

García-Altés A, Pérez K, Novoa A, Suelves JM, Bernabeu M, Vidal J, Arrufat V, Santamariña-Rubio E, Ferrando J, Cogollos M, Cantera CM, Luque JC (2012) Spinal cord injury and traumatic brain injury: a cost-of-illness study. Neuroepidemiology 39:103-108.

Ghatas MP, Lester RM, Khan MR, Gorgey AS (2018) Semi-automated segmentation of magnetic resonance images for thigh skeletal muscle and fat using threshold technique after spinal cord injury. Neural Regen Res 13:1787-1795.

Han Q, Jin W, Xiao Z, Ni H, Wang J, Kong J, Wu J, Liang W, Chen L, Zhao Y, Chen B, Dai J (2010) The promotion of neural regeneration in an extreme rat spinal cord injury model using a collagen scaffold containing a collagen binding neuroprotective protein and an EGFR neutralizing antibody. Biomaterials 31:9212-9220.

Han Q, Sun W, Lin H, Zhao W, Gao Y, Zhao Y, Chen B, Xiao Z, Hu W, Li Y, Yang B, Dai J (2009) Linear ordered collagen scaffolds loaded with collagen-binding brain-derived neurotrophic factor improve the recovery of spinal cord injury in rats. Tissue Eng Part A 15:2927-2935.

Han S, Wang B, Jin W, Xiao Z, Chen B, Xiao H, Ding W, Cao J, Ma F, Li X, Yuan B, Zhu T, Hou X, Wang J, Kong J, Liang W, Dai J (2014) The collagen scaffold with collagen binding BDNF enhances functional recovery by facilitating peripheral nerve infiltrating and ingrowth in canine complete spinal cord transection. Spinal Cord 52:867-873.

Han S, Wang B, Jin W, Xiao Z, Li X, Ding W, Kapur M, Chen B, Yuan B, Zhu T, Wang H, Wang J, Dong Q, Liang W, Dai J (2015) The linear-ordered collagen scaffold-BDNF complex significantly promotes functional recovery after completely transected spinal cord injury in canine. Biomaterials 41:89-96.

Han S, Xiao Z, Li X, Zhao H, Wang B, Qiu Z, Li Z, Mei X, Xu B, Fan C, Chen B, Han J, Gu Y, Yang H, Shi Q, Dai J (2018) Human placenta-derived mesenchymal stem cells loaded on linear ordered collagen scaffold improves functional recovery after completely transected spinal cord injury in canine. Sci China Life Sci 61:2-13.

Harness ET, Yozbatiran N, Cramer SC (2008) Effects of intense exercise in chronic spinal cord injury. Spinal Cord 46:733-737.

Hu SL, Luo HS, Li JT, Xia YZ, Li L, Zhang LJ, Meng H, Cui GY, Chen Z, Wu N, Lin JK, Zhu G, Feng H (2010) Functional recovery in acute traumatic spinal cord injury after transplantation of human umbilical cord mesenchymal stem cells. Crit Care Med 38:2181-2189.

Jiang J, Dai C, Niu X, Sun H, Cheng S, Zhang Z, Zhu X, Wang Y, Zhang T, Duan F, Chen X, Zhang S (2018) Establishment of a precise novel brain trauma model in a large animal based on injury of the cerebral motor cortex. J Neurosci Methods 307:95-105.

Kadoya K, Tsukada S, Lu P, Coppola G, Geschwind D, Filbin MT, Blesch A, Tuszynski MH (2009) Combined intrinsic and extrinsic neuronal mechanisms facilitate bridging axonal regeneration one year after spinal cord injury. Neuron 64:165-172.

Li X, Han J, Zhao Y, Ding W, Wei J, Han S, Shang X, Wang B, Chen B, Xiao Z, Dai J (2015) Functionalized collagen scaffold neutralizing the myelin-inhibitory molecules promoted neurites outgrowth in vitro and facilitated spinal cord regeneration in vivo. ACS Appl Mater Interfaces 7:13960-13971.

Li X, Han J, Zhao Y, Ding W, Wei J, Li J, Han S, Shang X, Wang B, Chen B, Xiao Z, Dai J (2016) Functionalized collagen scaffold implantation and cAMP administration collectively facilitate spinal cord regeneration. Acta Biomater 30:233-245.

Li X, Tan J, Xiao Z, Zhao Y, Han S, Liu D, Yin W, Li J, Li J, Wanggou S, Chen B, Ren C, Jiang X, Dai J (2017a) Transplantation of hUC-MSCs seeded collagen scaffolds reduces scar formation and promotes functional recovery in canines with chronic spinal cord injury. Sci Rep 7:43559.

Li X, Xiao Z, Han J, Chen L, Xiao H, Ma F, Hou X, Li X, Sun J, Ding W, Zhao Y, Chen B, Dai J (2013) Promotion of neuronal differentiation of neural progenitor cells by using EGFR antibody functionalized collagen scaffolds for spinal cord injury repair. Biomaterials 34:5107-5116.

Li X, Zhao Y, Cheng S, Han S, Shu M, Chen B, Chen X, Tang F, Wang N, Tu Y, Wang B, Xiao Z, Zhang S, Dai J (2017b) Cetuximab modified collagen scaffold directs neurogenesis of injury-activated endogenous neural stem cells for acute spinal cord injury repair. Biomaterials 137:73-86.

Lin H, Chen B, Wang B, Zhao Y, Sun W, Dai J (2006) Novel nerve guidance material prepared from bovine aponeurosis. J Biomed Mater Res A 79:591-598.

Liu F, Yang L, Liu J, Zhao Y, Xiao Z, Zheng Y, Xing Z, Zhang Y, Cao D (2019) Evaluation of hyperbaric oxygen therapy for spinal cord injury in rats with different treatment course using diffusion tensor imaging. Spinal Cord 57:404-411.

Liu T, Houle JD, Xu J, Chan BP, Chew SY (2012) Nanofibrous collagen nerve conduits for spinal cord repair. Tissue Eng Part A 18:1057-1066.

Maier IC, Schwab ME (2006) Sprouting, regeneration and circuit formation in the injured spinal cord: factors and activity. Philos Trans R Soc Lond B Biol Sci 361:1611-1634.

Momose H, Kashiwai H, Kawata Y, Hirayama A, Hirata N, Yamada K, Yamamoto M, Hirao Y (1997) Difference between the clinical significance of Credé voiding and Valsalva voiding in the urological management of spina bifida patients. Hinyokika Kiyo 43:771-775.

Noh MY, Lim SM, Oh KW, Cho KA, Park J, Kim KS, Lee SJ, Kwon MS, Kim SH (2016) Mesenchymal stem cells modulate the functional properties of microglia via TGF-β secretion. Stem Cells Transl Med 5:1538-1549.

Oh SK, Choi KH, Yoo JY, Kim DY, Kim SJ, Jeon SR (2016) A phase III clinical trial showing limited efficacy of autologous mesenchymal stem cell therapy for spinal cord injury. Neurosurgery 78:436-447.

Olby NJ, De Risio L, Muñana KR, Wosar MA, Skeen TM, Sharp NJ, Keene BW (2001) Development of a functional scoring system in dogs with acute spinal cord injuries. Am J Vet Res 62:1624-1628.

Orive G, Anitua E, Pedraz JL, Emerich DF (2009) Biomaterials for promoting brain protection, repair and regeneration. Nat Rev Neurosci 10:682-692.

Park JH, Kim DY, Sung IY, Choi GH, Jeon MH, Kim KK, Jeon SR (2012) Long-term results of spinal cord injury therapy using mesenchymal stem cells derived from bone marrow in humans. Neurosurgery 70:1238-1247.

Poplawski MM, Alizadeh M, Oleson CV, Fisher J, Marino RJ, Gorniak RJ, Leiby BE, Flanders AE (2019) Application of diffusion tensor imaging in forecasting neurological injury and recovery after human cervical spinal cord injury. J Neurotrauma 36:3051-3061.

Profyris C, Cheema SS, Zang D, Azari MF, Boyle K, Petratos S (2004) Degenerative and regenerative mechanisms governing spinal cord injury. Neurobiol Dis 15:415-436.

Properzi F, Carulli D, Asher RA, Muir E, Camargo LM, van Kuppevelt TH, ten Dam GB, Furukawa Y, Mikami T, Sugahara K, Toida T, Geller HM, Fawcett JW (2005) Chondroitin 6-sulphate synthesis is up-regulated in injured CNS, induced by injury-related cytokines and enhanced in axon-growth inhibitory glia. Eur J Neurosci 21:378-390.

Rajasekaran S, Kanna RM, Shetty AP (2012) Diffusion tensor imaging of the spinal cord and its clinical applications. J Bone Joint Surg Br 94:1024-1031.

Ritfeld GJ, Patel A, Chou A, Novosat TL, Castillo DG, Roos RA, Oudega M (2015) The role of brain-derived neurotrophic factor in bone marrow stromal cell-mediated spinal cord repair. Cell Transplant 24:2209-2220.

Rivlin AS, Tator CH (1977) Objective clinical assessment of motor function after experimental spinal cord injury in the rat. J Neurosurg 47:577-581.

Ruff CA, Wilcox JT, Fehlings MG (2012) Cell-based transplantation strategies to promote plasticity following spinal cord injury. Exp Neurol 235:78-90.

Schwab ME, Brösamle C (1997) Regeneration of lesioned corticospinal tract fibers in the adult rat spinal cord under experimental conditions. Spinal Cord 35:469-473.

Selvarajah S, Hammond ER, Haider AH, Abularrage CJ, Becker D, Dhiman N, Hyder O, Gupta D, Black JH 3rd, Schneider EB (2014) The burden of acute traumatic spinal cord injury among adults in the united states: an update. J Neurotrauma 31:228-238.

Snider S, Cavalli A, Colombo F, Gallotti AL, Quattrini A, Salvatore L, Madaghiele M, Terreni MR, Sannino A, Mortini P (2017) A novel composite type I collagen scaffold with micropatterned porosity regulates the entrance of phagocytes in a severe model of spinal cord injury. J Biomed Mater Res B Appl Biomater 105:1040-1053.

Sun X, Liu XZ, Wang J, Tao HR, Zhu T, Jin WJ, Shen KP (2020) Changes in neurological and pathological outcomes in a modified rat spinal cord injury model with closed canal. Neural Regen Res 15:697-704.

Theodore N, Hlubek R, Danielson J, Neff K, Vaickus L, Ulich TR, Ropper AE (2016) First human implantation of a bioresorbable polymer scaffold for acute traumatic spinal cord injury: a clinical pilot study for safety and feasibility. Neurosurgery 79:E305-312.

Tu Y, Chen C, Sun HT, Cheng SX, Liu XZ, Qu Y, Li XH, Zhang S (2012) Combination of temperature-sensitive stem cells and mild hypothermia: a new potential therapy for severe traumatic brain injury. J Neurotrauma 29:2393-2403.

Wang N, Xiao Z, Zhao Y, Wang B, Li X, Li J, Dai J (2018) Collagen scaffold combined with human umbilical cord-derived mesenchymal stem cells promote functional recovery after scar resection in rats with chronic spinal cord injury. J Tissue Eng Regen Med 12:e1154-1163.

Xiao Z, Tang F, Tang J, Yang H, Zhao Y, Chen B, Han S, Wang N, Li X, Cheng S, Han G, Zhao C, Yang X, Chen Y, Shi Q, Hou S, Zhang S, Dai J (2016) One-year clinical study of NeuroRegen scaffold implantation following scar resection in complete chronic spinal cord injury patients. Sci China Life Sci 59:647-655.

Xiao Z, Tang F, Zhao Y, Han G, Yin N, Li X, Chen B, Han S, Jiang X, Yun C, Zhao C, Cheng S, Zhang S, Dai J (2018) Significant improvement of acute complete spinal cord injury patients diagnosed by a combined criteria implanted with neuroregen scaffolds and mesenchymal stem cells. Cell Transplant 27:907-915.

Xu B, Zhao Y, Xiao Z, Wang B, Liang H, Li X, Fang Y, Han S, Li X, Fan C, Dai J (2017) A dual functional scaffold tethered with EGFR antibody promotes neural stem cell retention and neuronal differentiation for spinal cord injury repair. Adv Healthc Mater doi: 10.1002/adhm.201601279.

Zhang Q, Shi B, Ding J, Yan L, Thawani JP, Fu C, Chen X (2019) Polymer scaffolds facilitate spinal cord injury repair. Acta Biomater 88:57-77.

Zhao Y, Tang F, Xiao Z, Han G, Wang N, Yin N, Chen B, Jiang X, Yun C, Han W, Zhao C, Cheng S, Zhang S, Dai J (2017) Clinical study of neuroregen scaffold combined with human mesenchymal stem cells for the repair of chronic complete spinal cord injury. Cell Transplant 26:891-900.